JOURNAL OF MATERIALS SCIENCE 17 (1982) 264–276

Fatigue behaviour of metallic fibre-reinforced materials: a study of steel fibre-reinforced silver

Part 1 *Low-cycle fatigue*

G. ROSENKRANZ, V. GEROLD
Max-Planck-Institut für Metallforschung, Institut für Werkstoffwissenschaften, and Institut für Metallkunde, Universität Stuttgart, Federal Republic of Germany

D. STÖCKEL, L. TILLMANN
G. Rau, Pforzheim, Federal Republic of Germany

Low-cycle fatigue tests were performed on silver matrix–steel-fibre-reinforced composites (FRC) with unidirectionally aligned fibres of constant volume-fraction, $V_f = 0.35$. The influence of various material parameters, namely the fibre and matrix strengths, the interfacial bond strength and the mean fibre diameter, was examined. Low-cycle fatigue hardening and softening of FRCs deviate from the behaviour expected from the properties of the components. The differences are mainly based on a specific deformation or recrystallization structure of the composite matrix. The shapes of the stress–strain hysteresis loops are discussed qualitatively and compared to the experimental results. The comparison of fatigue life for different material conditions shows that the design of low-cycle fatigue-resistant metallic-fibre composites requires material criteria similar to those known to be responsible for high ultimate tensile strengths. The criteria may be varied if the composites are subjected to high-cycle fatigue loading.

1. Introduction

For general use of fibre-reinforced composites (FRC) as a new group of structural materials it is insufficient only to prove high factors of matrix reinforcement in static tensile strength. Since fatigue has generally turned out to be the most frequent cause of service failure, great emphasis has been placed on this subject during the past fifteen years. Most of the studies were performed on so-called state-of-the-art composites or model composites (e.g. [1–5]). The expected increase of matrix fatigue resistance by the introduction of high-strength fibres parallel to the main loading axis was based on two properties: firstly the high endurance limit of the fibres, which should act proportionally to the fibre volume-fraction, V_f, and secondly a possible modification of the matrix cyclic stress–strain behaviour and fatigue crack propagation as a result of joining the components. Several authors considered composites with brittle ceramic or less ductile metallic fibres, and demonstrated that complex damage and a great variety of crack propagation modes may appear during fatigue tests of this group of composites. Differences in the observed behaviour depended not only on the specific combination of components and on the fibre volume-fraction, but also on the composite structure and the properties of the fibre–matrix interface [1, 6].

The present investigation of the silver matrix–steel fibre system should promote the understanding of those factors which control different fatigue behaviours in a composite system with constant fibre volume-fraction. In addition, the selected combination represents those systems

0022–2461/82/010264–13$03.30/0

with comparable matrix and fibre ductility which have been partly neglected in the past. The model system is considered as quite suitable because many of those parameters which may influence the fatigue behaviour can be varied easily by the production process and subsequent heat treatments. It should be noted that similar metallic fibre-reinforced materials, e.g. the silver matrix–nickel fibre combination, are now used in electrical contact applications [7].

Part 1 of this study deals with low-cycle fatigue, that is, with high cyclic stress amplitudes which lead to failure of the FRC within some 10^5 cycles. Part 2 considers the high-cycle fatigue behaviour of the silver–steel composites up to 10^8 cycles to failure. The description of the fatigue damage development and different failure mechanisms will mainly be the subject of the second part.

2. Experimental procedure

2.1. Material fabrication and treatment

The silver–steel composites were made from silver (99.95 wt%) and the austenitic steel X 3 CrNi18/9(AISI 304 L). The combination exhibits an excellent chemical compatibility up to high temperatures; no formation of intermetallic phases is to be expected as the mutual solubility of silver and iron, chromium and nickel remains very low [7]. The composites were produced by a so-called indirect manufacturing method, namely the simultaneous drawing of silver-coated steel wires with subsequent heat treatments. The technique has been described in detail elsewhere [8]. Two different fibre diameters of approximately 35 μm and 200 μm were chosen and the fibre volume-fraction, V_f, was kept constant at 35%. Different degrees of cold work and recrystallization of the matrix enabled the fibre and matrix strengths to be changed. Regularly arranged points of weakness (multiple necking and fibre cracks) were introduced into the fibres by severe cold working (80% reduction in area) [9]. The fibre–matrix interfacial bond could be weakened by *in situ* oxidation of the steel fibre surfaces. To obtain the oxide-coated fibres the samples had to be annealed for a long time in oxygen. In materials with thick (200 μm) fibres the oxidation process ran from the surface through the whole specimen. In composites with thin (35 μm) filaments the process had to be stopped when 30% to 50% of the fibres were coated by an oxide layer. This interruption was necessary because increasing growth of the oxide film thickness, instead of the volume-fraction of the oxidized region of the sample, could be observed when the heat treatment was continued. For comparison, unreinforced silver rods were fabricated and heat treated in the same way.

The nomenclature of the different materials in this study, their degree of cold working, heat treatments and ultimate tensile strengths are given in Table I. Figs 1 to 4 show the microstructure of the materials. The transverse sections of FRC with thin fibres show the difference between the 30% and 80% pre-deformed material: the lower cold forming yields only little scatter of the fibre sectional areas (Fig. 1), whereas after severe cold forming fibre necking and cracking result in a wide scatter (Fig. 2). Though, after identical degrees of cold working, the difference is less pronounced in materials with 200 μm fibres (Figs 3 and 4), multiple necking and fibre fracture are nevertheless visible, as shown in Fig. 4, after chemical dissolution of the matrix. The ultimate tensile strengths of all composite states were determined in preliminary investigations. Experimental results never matched with those calculated from the simple rule of mixtures (ROM) by using the component properties. Extraordinarily small values, if compared with the ROM, emerged after recrystallization of the matrix in 80% pre-deformed FRC with thin fibres, and after *in situ* oxidation of the steel-fibre surfaces independent of the fibre diameter (Table I). In both materials the behaviour has been related to the fact that the mutual distances between fibre neckings approach the so-called critical aspect ratio l_c/d (l_c: critical length, d: fibre diameter). In this case the fibres cannot be loaded up to their ultimate tensile strength, but are pulled out of the matrix [10].

2.2. Testing

Samples were formed and polished on a copying lathe from as-drawn FRCs and unreinforced silver rods. The FRC specimen surfaces revealed lontitudinally cut fibres embedded in the silver matrix (Fig. 5). The different heat treatments are compiled in Table I.

The low-cycle fatigue tests were total-strain controlled and performed on a servohydraulic fatigue machine. All testing was done in tension–compression with zero mean load, using a sinusoidal wave-form. Cyclic loading was applied at a frequency of 10 Hz and decreased from time to time

TABLE I Data for tested composites and unreinforced silver

Material	Mean filament diameter (μm)	Degree of pre-deformation, $\psi = \frac{A_0 - A}{A_0} \times 100\%$	Heat treatment after fabrication	Ultimate tensile strength, σ_{uts}(MPa)
Composites				
Ag/St(g/30)	200	30	–	453
Ag/St(g/30/500° C)	200	30	500° C, 2 h in inert gas; matrix recrystallized	354
Ag/St(g/30/Ox)	200	30	500° C, 50(29†) days in air; matrix recrystallized, oxide-coated fibres (100%)	410
Ag/St(k/30)	30–40	30	–	465
Ag/St(k/30/500° C)	30–40	30	500° C, 2 h in inert gas; matrix recrystallized	425
Ag/St(k/30/Ox)	30–40	30	500° C, 38(14†) days in air; matrix recrystallized, oxide-coated fibres (30%, 50%†)	406
Ag/St(g/80)	200*	80	–	678
Ag/St(g/80/500° C)	200*	80	500° C, 2 h in inert gas; matrix recrystallized	523
Ag/St(g/80/Ox)	200*	80	500° C, 32(22†) days in air; matrix recrystallized, oxide-coated fibres (100%)	485
Ag/St(k/80)	0–50	80	–	605
Ag/St(k/80/500° C)	0–50	80	500° C, 2 h in inert gas; matrix recrystallized	413
Ag/St(k/80/Ox)	0–50	80	500° C, 31(10†) days in air; matrix recrystallized, oxide-coated fibres (30%, 50%†)	416
Unreinforced silver				
Ag(30)	–	30	–	254
Ag(30/500° C)	–	30	500° C, 2 h in inert gas; material recrystallized	158
Ag(80)	–	80	–	343
Ag(80/500° C)	–	80	500° C, 2 h in inert gas; material recrystallized	169

*Mean diameter in cross-sections without necking.
†Specimens tested at 20 000 Hz (see Part 2).

to 0.1 Hz in order to write hysteresis loops on an x–y plotter. Peak values of load and elongation were continuously recorded. The Stage I Young's modulus of the FRC (E_{cI}, fibres and matrix are deformed elastically). was electronically compensated for registration of "plastic" hysteresis loops.*

3. Results

3.1. Cyclic stress–strain behaviour

Silver–steel FRC and unreinforced silver specimens were fatigued to failure at two different total-strain amplitudes ($\Delta\epsilon^1_{tot} = 0.52\%$ and $\Delta\epsilon^2_{tot} = 0.8\%$). The lower amplitude, corresponding to the behaviour of the FRC components, leads to elastic–plastic matrix deformation and macroscopically elastic fibre loading in the undamaged material. On the other hand, the higher strain amplitude should result in a little plasticity of the reinforcing fibres as well. Fig. 6a shows the cyclic stress–strain behaviour of 80% pre-deformed specimens with thick fibres and a total strain amplitude of 0.52%, and Fig. 6b the behaviour of 30% pre-deformed samples with thin fibres and a strain amplitude of

*Young's modulus compensation of FRCs generally results in both overcompensation of the fibre modulus and incomplete componsation of the matrix modulus, or vice versa. Hence, from the resulting hysteresis loops no direct evidence emerges for the amount of plastic deformation of fibres or matrix.

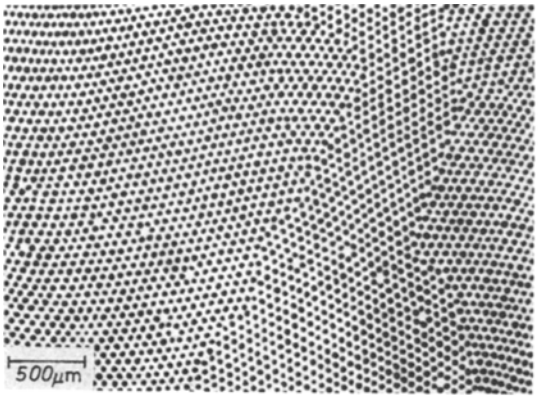

Figure 1 Transverse section of 30% cold-drawn Ag–steel FRC with thin (30–40 μm) fibres.

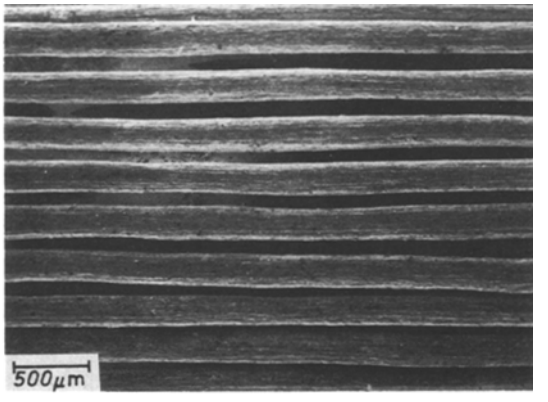

Figure 3 Steel fibres of 30% cold-drawn Ag–steel FRC after chemical dissolution of the silver matrix.

0.8%. For comparison, the behaviour of corresponding unreinforced silver is also included.

3.1.1. The initial test stage

In the as-drawn condition as well as after recrystallization of the matrix all FRC qualitatively behave like the unreinforced silver, i.e., the amount of softening or hardening per cycle of the deformed or recrystallized material, respectively, decreases during the test. The stress amplitude gradually approaches a constant value.

A more detailed analysis from the beginning of the test ($N = 20 \ldots 30$) up to a range of cycles with only little variation of the cyclic stress response ($N = 2.0 \ldots 3.0 \times 10^4$) for the unreinforced silver $[\Delta(\Delta\sigma^{Ag})]$ and the silver matrix $[\Delta(\Delta\sigma^{c})/(1 - V_f)]$ in the FRC reveals that the amounts of hardening of the recrystallized and of softening of the pre-deformed matrix never come up to the corresponding values of the unreinforced silver (Table II). For this calculation pure elastic fibre deformation has to be assumed. This seems to be quite reasonable, during the test stage in consideration, if the lower total strain amplitude $\Delta\epsilon^{I}_{tot}$ is chosen (Fig. 6a). If the fibres, too, are plastically deformed during testing an additional amount of softening of the pre-deformed fibres has to be taken into account. Consequently, despite matrix recrystallization a softening of the FRC from the beginning of the fatigue test was observed at high strain amplitudes (Fig. 6b).

In composites with oxide-coated filaments a behaviour similar to that described above for materials with recrystallized matrix was expected. In both cases the fibres remain in the pre-deformed condition after heat treatment while the matrix passes through the process of recrystallization. However, the observed differences cannot be explained merely by the modification of the fibre–matrix interfacial bond after *in situ*

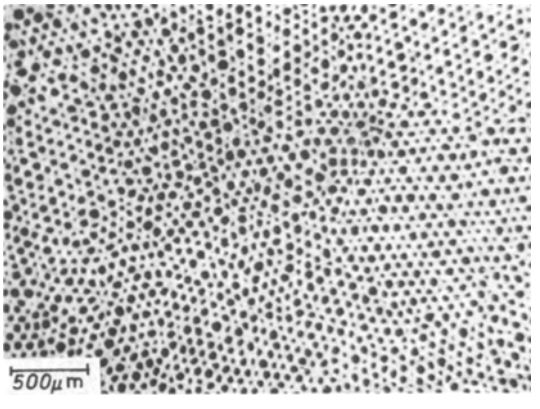

Figure 2 Transverse section of 80% cold-drawn Ag–steel FRC with thin (0–50 μm) fibres.

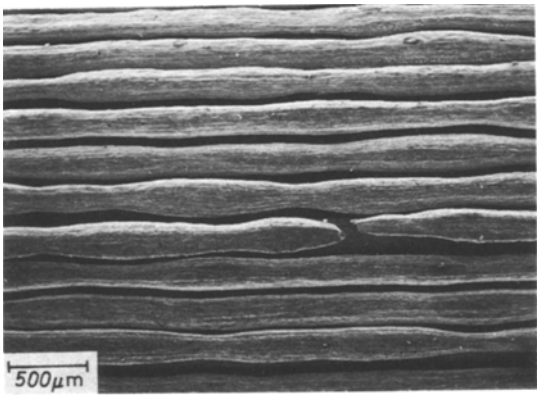

Figure 4 Steel fibres of 80% cold-drawn Ag–steel FRC after chemical dissolution of the silver matrix; multiple necking and fibre fracture result from the severe pre-deformation.

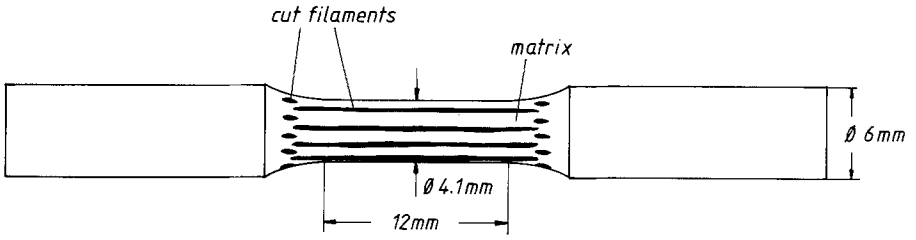

Figure 5 Shape of specimens for low-cycle fatigue tests.

oxidation of the steel fibre surfaces. The remarkable high initial fatigue stress amplitude of *in situ* oxidized FRC sample may serve as a first indication of the extensive consequences resulting from long-time heat treatment in the presence of oxygen (Figs 6a and b). In the fully oxidized condition of all fibre surfaces (thick fibres, Fig. 6a) the initial stress amplitudes are obviously higher than in materials with recrystallized matrix only. During fatigue testing, contrary to an expected initial hardening, the FRC immediately starts to soften, irrespective of the set strain amplitude

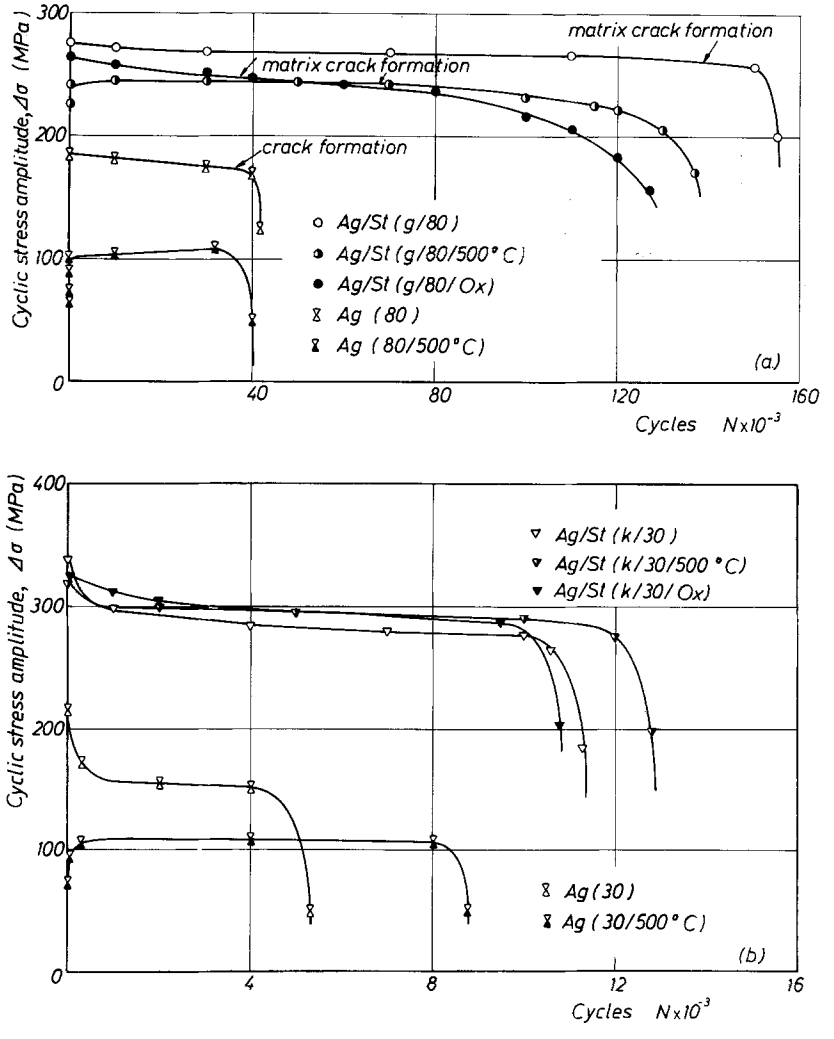

Figure 6 Typical cyclic hardening and softening curves of Ag–steel FRC and corresponding silver specimens. (a) 80% cold-drawn composites with thick (200 μm) fibres, $\Delta\epsilon_{tot} = 0.52\%$; (b) 30% cold-drawn composites with thin fibres, $\Delta\epsilon_{tot} = 0.8\%$.

TABLE II Changes of the cyclic stress amplitude $\Delta(\Delta\sigma)$ during the initial test stage in Ag–steel FRC and unreinforced silver; controlled strain amplitude $\Delta\epsilon^{I}_{tot} = 0.52\%$

Material	Interval of cycles, $N_1 \ldots N_2$ ($\times 10^{-4}$)	$\Delta(\Delta\sigma^{Ag})$; $\Delta(\Delta\sigma^{c})/(1 - V_f)$ (MPa)
Ag(30)	20 . . . 2	− 124
Ag/St(g/30)	20 . . . 2	− 105
Ag/St(k/30)	20 . . . 2	− 74
Ag(80)	30 . . . 3	− 23
Ag/St(g/80)	30 . . . 3	− 20
Ag/St(k/80)	30 . . . 3	− 17
Ag(30/500° C)	20 . . . 3	+ 56
Ag/St(g/30/500° C)	20 . . . 3	+ 43
Ag/St(k/30/500° C)	20 . . . 3	+ 25
Ag/St(g/30/Ox)	20 . . . 3	− 50*
Ag/St(k/30/Ox)	20 . . . 3	− 6*
Ag(80/500° C)	20 . . . 3.2	+ 91
Ag(g/80/500° C)	20 . . . 3.2	+ 57
Ag(k/80/500° C)	20 . . . 3.2	+ 60
Ag(g/80/Ox)	20 . . . 3.2	− 38*
Ag(k/80/Ox)	20 . . . 3.2	+ 38*

*Influence of the *in situ* oxidation of the steel–fibre surfaces.

(Fig. 6a, Table II). This tendency, initial softening instead of hardening, can be determined in all *in situ* oxidized silver–steel composites. However, in materials with thin filaments, where the surfaces of the fibres are only partly oxidized, the superimposed hardening of the recrystallized matrix may make the predominant contribution (Table II).

3.1.2. Stress–strain behaviour after the initial test stage

Following the initial hardening/softening test stage the cyclic curves exhibit either an almost constant value of the stress amplitude during cycling with the lower strain amplitude or a steady but little decrease when tested with the higher amplitude. This stage lasts up to more than 90% of the total lifetime and is followed by propagation of the final fatigue crack failure. This behaviour is similar to that of most conventional metallic materials.

Among all tested materials there are two striking exceptions (Fig. 6a):

(a) While the 80% pre-deformed material behaves as described above, the same composite after matrix recrystallization exhibits a constant stress amplitude value only up to 60% of its fatigue life ($N = 8 \times 10^4$ cycles); subsequently it starts to soften with increasing rate for a further 6×10^4 cycles to failure.

(b) After additional *in situ* oxidation of the fibre surfaces the material shows the same effect even more evidently: the initial softening in this material condition results in a steady decrease of the stress amplitude from the beginning of the test to failure.

In both cases the behaviour is caused by an early-starting fatigue damage of the silver matrix.

3.1.3. Hystersis behaviour

Though some problems of experimental and theoretical nature may arise from the description of cyclic elastic–plastic behaviour of FRC by hysteresis loops (see footnote, p. 266), it is considered to be helpful to examine the hysteresis shape and their qualitative modifications during fatigue loading. Fig. 7 shows the development of the loops of 80% pre-deformed silver–steel composites with 200 μm fibres fatigued at $\Delta\epsilon^{I}_{tot} = 0.52\%$. In heat-treated materials attention is attracted to a considerable deviation from elastic behaviour prior to complete unloading from either tension or compression. The effect is not observed during the initial test stage in 80% pre-deformed FRC (Fig. 7a, cycle number 55) but it develops during the observed fatigue-induced matrix softening (Fig. 7a, cycles number 10^4 and 7×10^4).

Initial matrix hardening in the recrystallized condition is proved by a decrease of loop width between cycle number 35 and 10^4 (Fig. 7b). Comparison of Figs 7b and c indicates that the

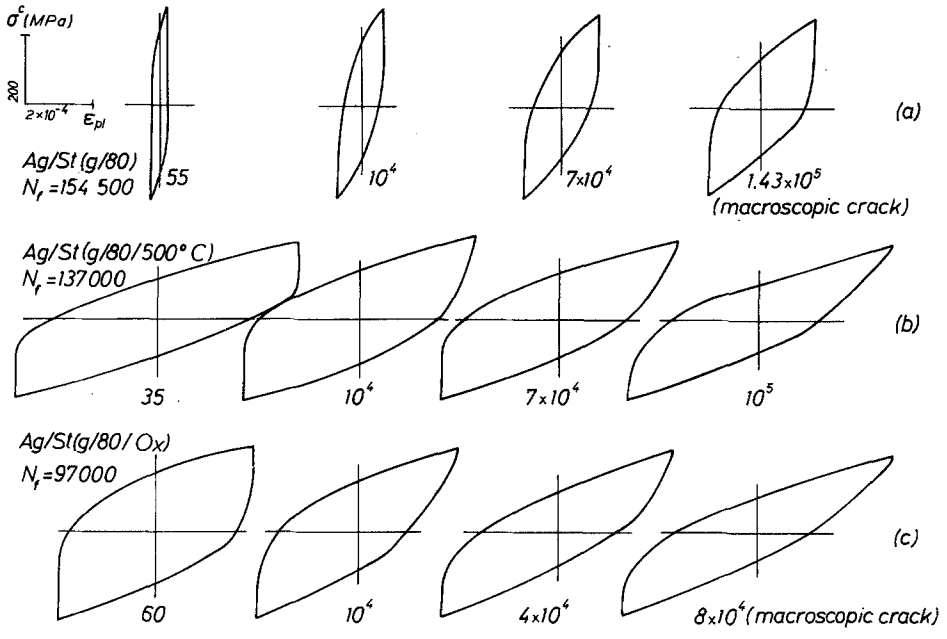

Figure 7 Development of experimental hysteresis loops during the fatigue tests (after E_{cI} compensation); FRC with 200 μm fibres, $\Delta\epsilon_{tot} = 0.52\%$. (a) 80% cold-drawn, (b) 80% cold-drawn, matrix recrystallized, (c) 80% cold-drawn, *in situ* oxidized fibre surfaces.

initial plastic strain amplitudes of FRC with recrystallized matrix are diminished by virtue of an additional *in situ* oxidation of the steel fibre surfaces.

Some well-defined material conditions cause extremely asymmetric changes of the hystesis loop shapes during fatigue testing. When unloaded from the tensile half-cycle, the Young's modulus of the specimen seems to drop gradually to lower values with increasing number of cycles. On the other hand, compressive half-cycles show only little variations in Young's modulus. The behaviour appears most evidently and relatively early during fatigue testing in composites with *in situ* oxidized fibre surfaces (Fig. 7c) (exception: 80% pre-deformed FRC with thin fibres) and in the 80% pre-deformed material with thick fibres after matrix recrystallization (Fig. 7b). The effect is more pronounced for lower total-strain amplitudes.

3.2. Low-cycle fatigue life

For a clear presentation it was decided to discuss low-cycle fatigue-life data on a stress-range basis in spite of the strain-controlled tests. For this purpose the cyclic stress amplitude at half-life of the materials $\Delta\sigma_h^c$ was plotted against the logarithm of the number of cycles to failure, N_f. All experimental results are compiled in this way in Fig. 8a and b, which show the diagrams of FRC with 200 μm and 35 μm filaments, respectively. Results from corresponding unreinforced silver are also included. Measured points of 30% pre-deformed FRC are collected in scatter bands.

The cyclic stress amplitudes of 80% pre-deformed FRC with thick fibres clearly exceed those of 30% cold-formed materials at the same low-cycle fatigue life (Fig. 8a). As was to be expected 80% pre-deformed composites with no further heat treatment show higher load amplitudes than those with a recrystallized matrix, i.e., a lowered yield strength. The difference of the stress amplitudes between heat-treated 30% and 80% pre-deformed FRC decreases with increasing fatigue life, leading to almost identical stress amplitudes of both groups of FRC at $\Delta\epsilon_{tot}^{I} = 0.52\%$ (lower group of measured points in Fig. 8a, $\Delta\sigma \approx 240$ MPa). The observation is not surprising because at this strain amplitude only elastic fibre behaviour can be assumed in all material conditions, while the heat-treated recrystallized matrix showed elastic–plastic deformation. On the other hand, high stress differences at the high strain amplitudes prove that 80% pre-deformed reinforcing fibres, in contrast to those only 30% cold worked, still show a macroscopically almost pure elastic deformation (see Section 3.1.1).

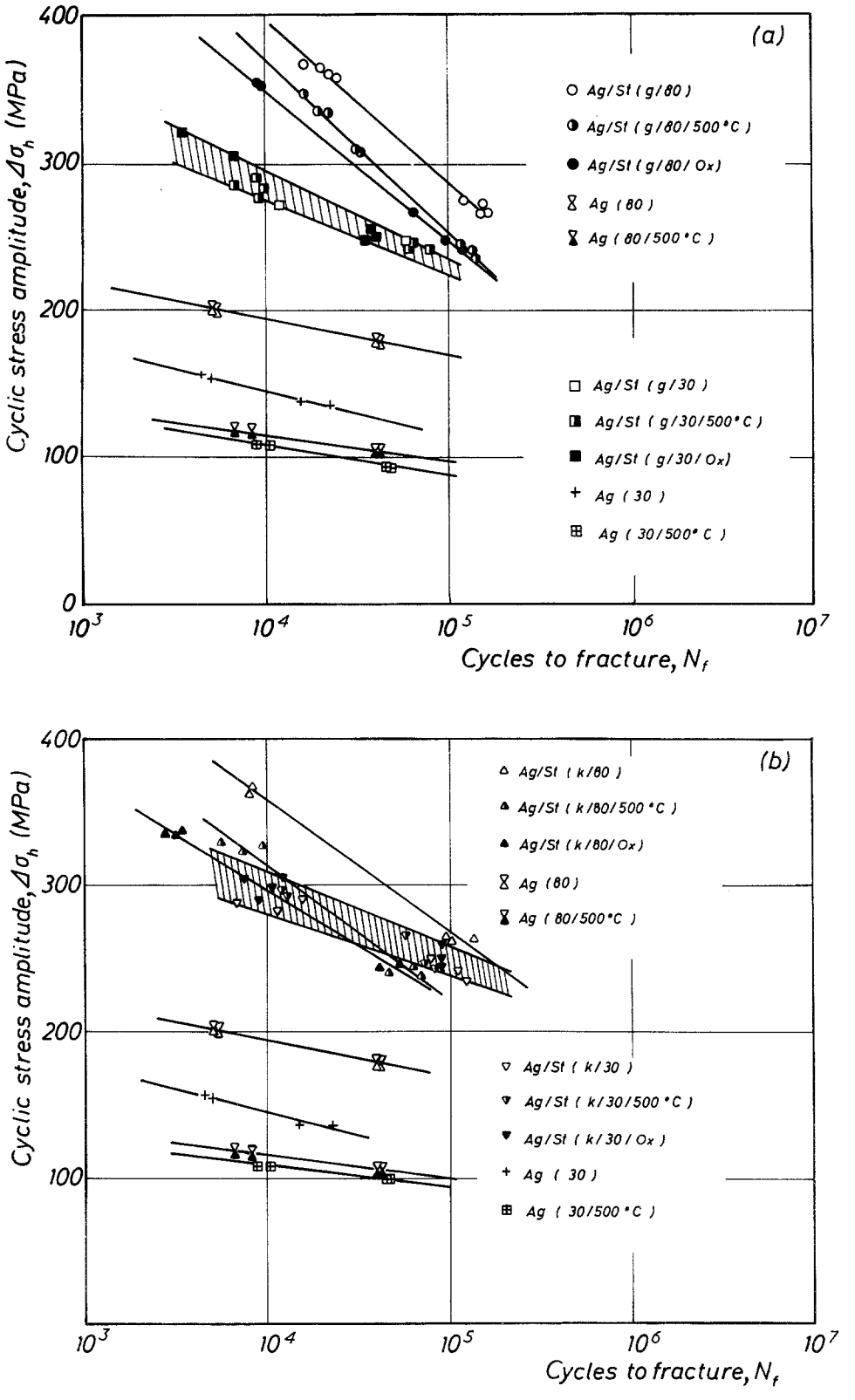

Figure 8 Cyclic stress amplitude at half-life of composites and bulk silver material plotted against the number of cycles to failure. (a) FRC containing thick (200 μm) fibres, (b) FRC containing thin (30–40 μm) fibres.

The behaviour of corresponding composites with thin fibres (Fig. 8b) does not differ very much from that discussed above. However, two details should be noted: firstly, measured points of 80% pre-deformed FRCs, especially after a heat treatment, are shifted to lower stress values if compared with Fig. 8a. Secondly, the scatter band of 30% pre-deformed composites is slightly raised. The former difference is due to the pronounced multiple necking and fibre discontinuities in the named material states; the latter may be related to mutual constraint effects of the two components, formerly reported by Stuhrke [11] and Kelly and Lilholt [12] for very fine structures.

4. Discussion

4.1. Cyclic stress–strain behaviour

In some conditions hardening and softening of silver–steel FRC considerably differs from what is expected in view of the properties of the composite components. At least, if loading of the reinforcing filaments remains elastic, the amounts of softening and hardening of the matrix are diminished in pre-deformed and in annealed (2 h/500° C) materials, respectively, if compared with identically treated and tested unreinforced silver. After *in situ* oxidation of all fibre surfaces, i.e., heat treatment at 500° C in oxygen, not only a quantitative but also a qualitative change was observed between the behaviour of the FRC and unreinforced, recrystallized silver. The FRC shows softening during the initial test stage instead of hardening which was expected because of the recrystallized matrix.

Introducing some simplifications, the width of an FRC hysteresis loop as a measure of plastic deformation of the material can be easily determined from properties of the components (see Section 4.2.). Without exception the calculated plastic strain amplitudes exceed those recorded during low-cycle fatigue experiments. All observations suggest that the ductility of the silver matrix is reduced when compared with that of unreinforced silver. As mentioned above, Stuhrke [11] and Kelly and Lilholt [12] explained a similar behaviour by mutual constraint effects of the two components caused by different Poisson's ratios of fibre and matrix. This effect, however, is restricted to the direct vicinity of the fibres and may be of secondary importance in the course structures used in this study [13]. In the present case we propose that differences between the structure state of the silver matrix and the unreinforced silver are mainly responsible for the observed fatigue characteristics.

4.1.1. Composites with recrystallized matrix

In a previous work it was reported that the same recrystallization treatment results in a clearly larger grain size in unreinforced silver than in the silver matrix of silver–steel composites [10]. Corresponding to the Hall–Petch relation

$$\sigma_y = \sigma_0 + kd^{-1/2}, \tag{1}$$

where σ_y is the yield strength, σ_0 and k are constants and d is the mean grain size, the yield strength of a metallic material increases when the grain size decreases; this leads to a smaller plastic strain amplitude during low-cycle fatigue. In silver, however, this contribution should be small, because of low values of the constant k in fcc metals.

In accordance with observations reported by Hancock and Grosskreutz [14] for aluminium alloy–stainless steel composites, slightly differing linear coefficients of thermal expansion between the filaments and the matrix may be of importance in the recrystallized material. During cooling down from the annealing temperature residual stresses are created in both components. An estimation of the possible residual stresses σ_r around the fibre can be made from the equation

$$\sigma_r = E_m(\alpha_f - \alpha_m)\Delta T, \tag{2}$$

where E_m is the Young's modulus of the matrix (8.2×10^4 MPa), α_f and α_m are the linear coefficients of thermal expansion for the fibre and the matrix [18×10^{-6} K^{-1} (0 . . . 400° C) and 21×10^{-6} K^{-1} (0 . . . 400° C), respectively] and ΔT is the temperature interval (400 K; dynamic recovery of the stresses between 500° C and 400° C is assumed). At room temperature this reveals tensile residual stresses of approximately 100 MPa in the matrix, which exceed the yield point of the recrystallized matrix ($\sigma_y^m \approx 65$ MPa). To reduce the residual stresses the matrix will deform plastically at least in a layer adjacent to the fibres. Comparison of the micro-Vickers pyramid hardnesses of the matrix of similar silver–steel composites and the unreinforced silver confirms this assumption (Table III).

TABLE III Microhardness of unreinforced silver and the silver matrix in FRCs

Material	(Heat) Treatment	Microhardness MHV (5p) (Kp mm^{-2})
Unreinforced silver	500° C, 2 h in argon	45
Silver matrix in FRC	500° C, 2 h in argon	50–57
Silver matrix in FRC	500° C, in air, no visible *in situ* oxidation	62–67
Silver matrix in FRC	500° C, in air, oxide-coated filaments	75–84.5
Silver matrix in FRC	30% cold formed	84.5

4.1.2. As-drawn composites

In this group of composites, which was not subjected to heat treatment, diminished softening compared to identically treated and fatigued unreinforced silver was also explained by the lower ductility of the silver matrix. But all reasons stated above in view of the recrystallized matrix materials obviously cannot hold in this case. A differing grain alignment (texture) of the silver matrix grains and those of the unreinforced material during fabrication may prove to be a possible explanation. For clarification, however, separate investigations are necessary.

4.1.3. In situ oxidized composites

The unexpected high initial stress amplitudes and softening of this group of materials, too, appears to be a combination of more than one effect:

(a) The contribution of different coefficients of thermal expansion described above should be accelerated by the formation of the oxide layer, since oxides usually show very low α_T [15].

(b) The oxygen incorporated in the silver matrix is not only used for variation of the fibre–matrix interfacial structure but also increases the yield strength of the bulk silver matrix [16, 17]. Hence a reduced plastic strain amplitude during fatigue testing is expected in silver–steel composites if compared with unreinforced silver recrystallized in an argon atmosphere.

(c) An increase of the FRC volume during oxidation (the specimen diameter was measured prior to heat treatment) results in an increase of the initial nominal stress amplitude.

Both the contribution of the differing coefficients of thermal expansion (a) and of oxygen (b) are again confirmed by the cited micro-hardness tests (Table III).

The initial fatigue softening of *in situ* oxidized silver–steel composites may now be explained as follows: matrix hardening is in whole or in part impeded by an increased matrix yield strength contribution of the oxygen incorporated in the silver lattice) and dislocation density (effect of differing coefficients of thermal expansion) prior to fatigue testing. Degradation and delamination of the brittle oxide layers and their gradual destruction are responsible for the initial softening. The SEM micrograph (Fig. 9) shows the edge of a hollow, which was left by a filament pulled out

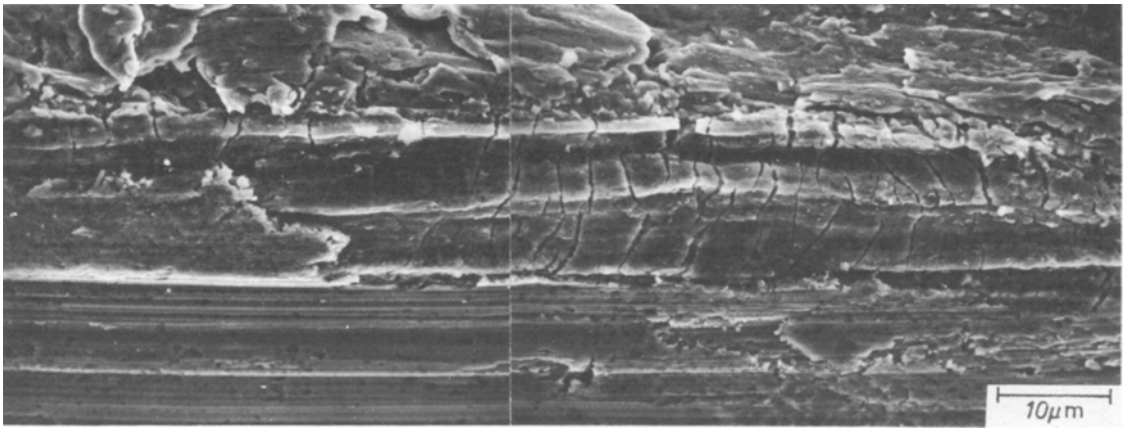

Figure 9 Multiple fracture of the interfacial oxide layer in *in situ* oxidized FRC; $\Delta\epsilon_{tot} = 0.52\%, N_f = 7.3 \times 10^4$ cycles.

during fatigue failure. A relatively strong bond between the reaction layer and the matrix causes the formation of equidistant oxide cracks during fatigue.

Moreover, another contribution, examined in detail by Ochiai *et al.* [18] using an aluminium–stainless steel system with a brittle zone at the fibre–matrix interface, may have an effect on the present observation. Ochiai *et al.* reported that brittle layers raise the tensile strength of the fibres as long as they adhere to the fibres and are not fractured by compressive transverse stresses. The present fatigue tests revealed a gradual delamination of the fibre–oxide layer interface during the initial test stage.

4.1.4. Hysteresis behaviour

To clarify the experimental shape of the stress–strain hysteresis, FRC loops were calculated by the rule of mixtures, which for this purpose had to be extended into the plastic matrix–elastic fibre region. Purely elastic filaments and an elastic–plastic matrix were assumed. Possible fibre–matrix interactions were neglected. Because of the inaccuracy of the experimental compensation of the Young's modulus E_{cI} in such composites,* it was not attempted to compare calculated and experimental diagrams quantitatively.

What follows is a discussion of the principal shape of the loops: FRC with different matrix properties produce the schematic, calculated loops plotted in Fig. 10 after compensation of the E_{cI} modulus. This example is based on the lower experimental total-strain amplitude $\Delta\epsilon^1_{tot} = 0.52\%$ and matrix yield strengths of 65 MPa for a recrystallized and 180 MPa for an 80% cold-worked matrix. Fig. 10 confirms the two types of loop shapes experimentally observed during the initial stage of the fatigue test (Fig. 7). The narrow loop (full line) in Fig. 10 reflects the experimental loop on the left side of Fig. 7a. The softening of this 80% pre-deformed composite during fatigue testing causes an approach of the loop shape to the calculated and experimentally-determined second loop (Fig. 10, broken line, and Figs 7b and c) of materials with a recrystallized matrix phase. This material condition shows the characteristic deviation from elastic behaviour prior to complete

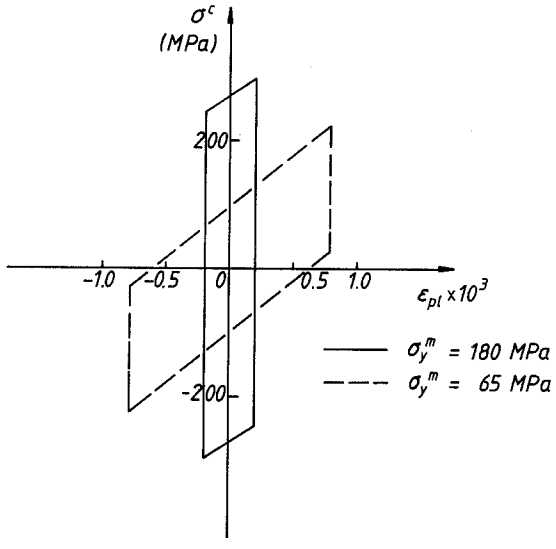

Figure 10 "Plastic" composite hysteresis loops after compensation of E_{cI} as calculated from the component properties for $\Delta\epsilon_{tot} = 0.52\%$; fibre volume-fraction $V_f = 0.35$, $E_f = 20 \times 10^4$ MPa, $E_m = 8.2 \times 10^4$ MPa, $E_{cI} = E_f V_f + E_m(1 - V_f) = 12.3 \times 10^4$ MPa; σ_y^m: matrix yield strength.

unloading of FRCs, based on a plastic matrix deformation in the opposite direction; i.e., the matrix experiences compressive plastic deformation before the reinforcing fibres and the composite are completely unloaded to zero stress from the tensile half-cycle and vice versa [19–21].

The development of asymmetric hysteresis loops in FRC resembles the shape changes observed in conventional metallic materials during fatigue crack propagation. In FRC the phenomenon is usually associated with a gradual decrease of the stress amplitude with increasing number of cycles (cf. Fig. 6a, heat-treated composite conditions). Stereo-microscopic observations of corresponding specimen surfaces during the fatigue tests reveal that the change of loop shape can be attributed to a gradual accumulation of damage which spreads far into the bulk material. The nucleation of several matrix cracks preceeds the propagation of the final fatigue crack and causes a reduction of the stress-bearing cross-section of the FRC. During unloading from the maximum tensile load, the effective Young's modulus based on the initial cross-section consequently drops down. On the other hand, the matrix crack surfaces are pressed

*The inaccuracy mainly depends on the difficulty of identifying the transition from Stage I (elastic filaments and matrix, E_{cI}) at the tensile stress–strain curve to Stage II (elastic filaments, plastic matrix, E_{cII}). Instead of two straight lines with different slopes one slightly curved line is determined during fatigue testing [10].

together during unloading from the maximum compressive load and this half-cycle consequently shows little difference of the actual Young's modulus compared to the modulus of the undamaged material.

Hence, changes of hysteresis loop shapes may serve as an indication of the development of severe fatigue damage in FRCs, before filament failure and propagation of the final fatigue crack.

4.2. Low-cycle fatigue life

To compare fatigue lifes of the FRC and the unreinforced matrix material, analyses based on the stress-range and on the strain-range have to be distinguished. If a stress-range analysis is favoured for the present fatigue experiments (Section 3.2., Fig. 8), the main influence on low-cycle fatigue resistance is attributed to the variation of the degree of cold work of the filaments and the matrix. The improvement of fatigue life by reinforcement (see Fig. 8) is expected and is mainly due to the mechanical properties of the stainless steel, i.e., the higher Young's modulus, yield strength and fatigue limit. If, on the other hand, the evaluation on a strain-range basis is preferred, that is, the behaviour of silver and identically treated silver–steel composites is compared at a fixed total strain amplitude, differences of the numbers of cycles to failure are not as self-evident as in the case before. The unreinforced silver and the silver matrix are cyclically loaded with identical total strain amplitudes. Then, to improve the fatigue resistance of the silver by the fibres, it is necessary either to delay crack nucleation in the matrix or to avoid fracture of the fibres during crack propagation.

In the low-cycle range the nucleation of matrix fatigue cracks usually results also in a quick nucleation of filament cracks and in subsequent composite failure. Hence, above all, the delay of matrix crack initiation determines the number of cycles to failure.

In the present investigation, delayed nucleation of critical matrix cracks was observed in predeformed silver–steel composites without further heat treatment and after matrix recrystallization. The delay is most likely caused by the decreased ductility of the silver as a component of the FRC. Consequently, in total-strain controlled fatigue tests the plastic strain amplitude is reduced compared to unreinforced silver. Critical matrix cracks form latest in severely cold-worked composites. For example, the nucleation of matrix cracks, visible in a stero-microscope (magnification 50×), was delayed by more than a factor of four in 80% pre-deformed composites with 200 μm filaments ($\Delta\epsilon^1 = 0.52\%$; see Fig. 6a).

An additional contribution to decreased matrix ductility, which may be expected in fine-structured FRCs, as a result of mutual constraint effects appears to be small in the fibre diameter range investigated. If actually existing, the effect is superimposed by severe multiple necking and fibre discontinuities in 80% pre-deformed composites with thin fibres (see Section 3.2, Fig. 8b). Namely, such fibre defects induce elevated local plastic strain amplitudes during fatigue loading in the surrounding matrix zone, leading to premature nucleation of fatigue cracks. Potential positive aspects of regularly spaced fibre necking in the present case and of points of filament weakness in general will be discussed in Part 2 of this paper.

No delay of matrix crack formation during low-cycle fatigue was found in composites with *in situ* oxidized fibre surfaces. Even premature crack formation, compared with corresponding unreinforced silver, was observed and attributed to the formation of internal notches, i.e., stress and strain concentrations, by cracking of the interface reaction layer during the initial test stage. This obviously overcompensates for the reduced ductility effects of the matrix, which also were observed in this material state.

The second source of potential improvement of the FRC fatigue resistance, the possibility of avoiding fracture of the fibres during crack propagation, gains in significance with decreasing strain or load amplitudes, especially near the fatigue limit. Nevertheless, low-cycle fatigue tests, too, revealed essential changes of fatigue damage mechanisms after appropriate heat treatment (Fig. 6a, 7b and c). However, this type of improvement is not sufficient to achieve the maximum fatigue resistance, which was observed in 80% pre-deformed FRC with no further heat treatment. Details will be presented in Part 2.

Following the above presentation some criteria for the design of low-cycle fatigue resistant composites of the silver–steel system as a model for similar metal–metal FRCs may be listed. We shall see that high cyclic stress and strain amplitudes lead to criteria, which are essentially identical with those developed for improved ultimate tensile strengths of unidirectional fibre reinforced composite

systems: high strength fibres and matrix, high interfacial bond strength, fine structure, e.g. small fibre diameters and small mutual fibre spacings [22], no fluctuations of the fibre strength along the filaments.

In practical operation very often the absolute fatigue life is not the only decisive criterion, but also the fatigue fracture toughness [6]. This will change some of the criteria cited above, as will be discussed in Part 2.

5. Conclusions

(a) Low-cycle fatigue hardening and softening of unidirectionally reinforced silver–steel fibrous composites with constant fibre volume-fraction ($V_f = 0.35$) deviate from the behaviour expected from the properties of the components. This deviation is essentially based on a specific deformation or recrystallization structure of the composite matrix differing from that of the unreinforced material. In heat-treated materials this is due to different coefficients of thermal expansion of the filaments, the matrix and, in the case of *in situ* oxidized materials, the oxide coating of the fibres. The oxygen penetration and the increase in volume during formation of the oxide layers, too, influence the behaviour in this material.

(b) Low-cycle fatigue life in composites with comparable fibre and matrix strengths and a strong interfacial bond is solely controlled by matrix fatigue crack formation. On the other hand, fatigue failure of the filaments and the composite may be preceeded by the accumulation of early matrix damage which gradually increases and fibre–matrix debonding in composites with extremely different fibre and matrix strengths and/or a weak interfacial bond.

(c) The shape of stress–strain hysteresis loops obtained from metallic fibre reinforced composites may be calculated by the simple rule of mixtures from the properties of the components. Good qualitative agreement with the principal experimental loop shapes of different material conditions was found. Asymmetric changes of the loop shape observed in some well-defined conditions are caused by crazing of the matrix and fibre–matrix interface and may serve as an indication for the accumulation of fatigue damage in fibre reinforced composites.

(d) The design of metallic fibre-reinforced composites which are resistant to low-cycle fatigue loading requires essentially the same criteria, which are known to be responsible for high ultimate tensile strengths.

(e) In the range covered by this investigation fibre diameters (approximately 35 μm to 200 μm) or mutual fibre spacings do not affect very much the low-cycle fatigue response. Constraint effects, reported to be important in very fine structured composites, obviously play only a secondary role in the present case.

References

1. J. R. HANCOCK, in "Composite Materials", Vol. 5: "Fracture and Fatigue" edited by L. J. Broutman (Academic Press, New York, 1974) p. 371.
2. A. A. BAKER, *J. Mater. Sci.* **3** (1968) 412.
3. A. A. BAKER, D. M. BRADDICK and R. W. JACKSON, *ibid.* **7** (1972) 747.
4. J. L. CHRISTIAN, in "Fatigue of Composite Materials", *ASTM STP* **569** (1975) p. 280.
5. M. A. McGUIRE and B. HARRIS, *J. Phys. D: Appl. Phys.* **7** (1974) 1803.
6. A. A. BAKER, *Appl. Mater. Res.* **5** (July 1966) 149.
7. M. HANSEN and K. ANDERKO, in "Constitution of Binary Alloys" (McGraw-Hill, New York, 1958) pp. 17, 20, 36.
8. D. STÖCKEL, *J. Mater. Technol. Test.* **10** (1979) 230.
9. G. ROSENKRANZ, D. STÖCKEL and L. TILLMANN, *ibid.* **7** (1976) 317.
10. *Idem, Z. Metall.* **69** (1978) 266.
11. W. F. STUHRKE, in "Metal Matrix Composites", *ASTM STP* **438** (1968) p. 108.
12. A. KELLY and H. LILHOLT, *Phil. Mag.* **20** (1969) 311.
13. K. K. CHAWLA, *J. Mater. Sci.* **10** (1975) 1831.
14. J. R. HANCOCK and J. C. GROSSKREUTZ, in "Metal Matrix Composites", *ASTM STP* **438** (1968) 134.
15. LANDOLT–BÖRNSTEIN, "Numerical Data and Functional Relationships in Science and Technology" New Series, Group III, Vol. 4a, b, edited by K. H. Hellwege (Springer-Verlag, Berlin 1970).
16. H. BÖHM, *Metall.* **17** (1963) 706.
17. M. AHLERS, *Z. Metall.* **56** (1965) 741.
18. S. OCHIAI and Y. MURAKAMI, *Trans. Japan Inst. Met.* **18** (1977) 384.
19. K. G. KREIDER and K. M. PREWO, in "Composite Materials", Vol. 4: "Metallic Matrix Composites", edited by K. G. Kreider (Academic Press, New York, 1974) p. 459.
20. G. J. DVORAK and J. Q. TARN, in "Fatigue of Composite Materials", *ASTM STP* **569** (1975) 145.
21. H. J. WEISS, *J. Mater. Sci.* **12** (1977) 797.
22. G. ROSENKRANZ, Thesis, Universität Stuttgart, FRG (1979).

Received 22 May
and accepted 18 June 1981